




Robust Directional Couplers for State Manipulation in Silicon Photonic-Integrated Circuits

Moshe Katzman, Yonatan Piasetzky , Evyatar Rubin, Ben Barenboim, Maayan Priel, Muhammed Erew, Avinoam Zadok , and Haim Suchowski 

(*Integrated Photonics 2022*)

Abstract—Photonic integrated circuits play a central role in current and future applications such as communications, sensing, ranging, and information processing. Photonic quantum computing will also likely require an integrated optics architecture for improved stability, scalability, and performance. Fault-tolerant quantum computing mandates very accurate and robust quantum gates. In this work, we demonstrate high-fidelity directional couplers for single-qubit gates in photonic integrated waveguides, utilizing a novel scheme of detuning-modulated composite segments. Specific designs for reduced sensitivity to wavelength variations and real-world geometrical fabrication errors in waveguide width and depth are presented. Enhanced wavelength tolerance is demonstrated experimentally. The concept shows great promise for scaling high fidelity gates as part of integrated quantum optics architectures.

Index Terms—Coherent control, directional couplers, integrated quantum photonics, quantum electronics, silicon photonics.

I. INTRODUCTION

PHOTONIC-INTEGRATED circuits (PICs) are essential for present and future data center communications [1]. PICs are also widely regarded among the most promising platforms for the realization of quantum technologies in computation, information processing, and sensing [2]–[5]. The advancement of quantum integrated photonics would critically depend on the reduction of errors [2], [4]. Compared with classical applications, quantum technologies are far less tolerant to possible uncertainties associated with the fabrication of PICs [6].

The directional coupler is among the most fundamental and widely employed building blocks of PICs [5]. Quantum photonic applications require that the splitting ratios of directional

couplers comply with a target design to the fourth decimal point [6]. This requirement places stringent tolerances on process parameters such as etching depth, waveguide widths, etc., which are difficult to meet in practice. Geometrical errors are often correlated: they affect both constituent waveguides in the directional coupler in the same manner. In addition, quantum-photonic integrated circuits would need to operate over ranges of wavelengths and temperatures, leading to further variations in their transfer functions. Unfortunately, standard directional couplers with uniform waveguide sections do not exhibit sufficient tolerance to inevitable fabrication and spectral uncertainties [5].

Much effort has been dedicated in recent years to the design and realization of robust photonic-integrated couplers and quantum gates [2], [7]–[9]. For example, several works have reported wavelength insensitive couplers in silicon-on-insulator (SOI) photonics [10]–[13]. However, fewer works addressed tolerance to geometrical errors in fabrication. Recently, some of us have proposed a design concept for fault-tolerant directional couplers based on waveguide sections of different widths [14]. The approach is based on the principles of composite pulse sequences used in atomic physics [15], [16]. The so-called composite-sections couplers are simple to realize, and they do not require modifications to the fabrication protocols. The design approach is generic and can be optimized for the mitigation of errors in wavelength or geometry.

In this work, we report composite-sections directional couplers in the standard SOI platform, the workhorse of PICs. One specific design addresses wavelength variations, whereas another provides enhanced tolerance to real-world geometrical fabrication errors in the widths and etching depth of both coupler waveguides. Improved spectral stability is demonstrated experimentally: the coupling ratios of hundreds of microns-long uniform and composite-sections couplers are characterized across the C-band wavelengths. The spectral sensitivity of the composite-sections couplers splitting ratio is reduced by over an order of magnitude. The composite-sections couplers may serve as a fundamental building block of practical quantum silicon photonics.

II. DESIGN OF COMPOSITE-SECTION DIRECTIONAL COUPLERS

According to the coupled-mode theory, the propagation of the pair of electrical fields $E_{1,2}$ in a directional coupler of a fixed

Manuscript received 25 February 2022; revised 3 May 2022; accepted 11 May 2022. Date of publication 13 May 2022; date of current version 16 December 2022. This work was supported by the Israel Science Foundation (ISF) quantum science and technology program under Grant 3427/2021. (Moshe Katzman and Yonatan Piasetzky contributed equally to this work.) (Corresponding author: Haim Suchowski.)

Moshe Katzman, Evyatar Rubin, Ben Barenboim, Maayan Priel, and Avinoam Zadok are with the Faculty of Engineering and the Institute for Nano-Technology and Advanced Materials, Bar-Ilan University, Ramat-Gan 5290002, Israel (e-mail: moshekatzman111@gmail.com; evyatar10.rubin@gmail.com; benb7243@gmail.com; lmaayanl@gmail.com; avinoam.zadok@biu.ac.il).

Yonatan Piasetzky, Muhammed Erew, and Haim Suchowski are with the Department of Condensed Matter Physics, School of Physics and Astronomy, Tel Aviv University, Tel Aviv 6997801, Israel (e-mail: piasetzky1@mail.tau.ac.il; muhammad.erew@gmail.com; haimsu@tauex.tau.ac.il).

Color versions of one or more figures in this article are available at <https://doi.org/10.1109/JLT.2022.3175128>.

Digital Object Identifier 10.1109/JLT.2022.3175128

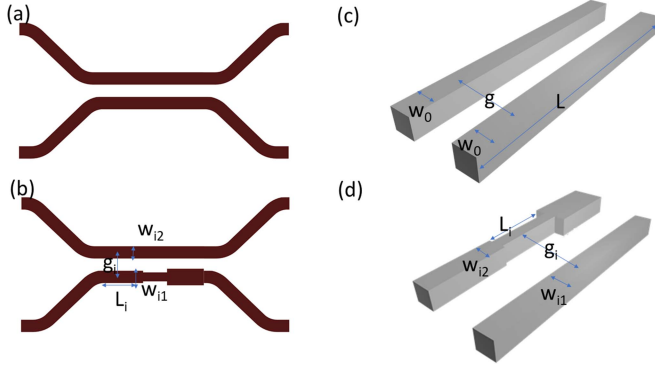


Fig. 1. Schematic illustrations of standard and composite-sections directional couplers. (a): Top view of a standard coupler with constant cross-section vs. a composite-sequence coupler (b), which has piecewise constant cross-section for any number of segments. Panels (c)-(d) Show a 3D view of the coupling region inside the standard and composite-sections couplers, respectively. The design parameters of waveguides widths, lengths, and gaps in the different segments are noted (see text).

cross-section is described by the following unitary propagator:

$$\begin{bmatrix} E_1(z) \\ E_2(z) \end{bmatrix} = \begin{bmatrix} \cos(A) + \frac{i\Delta\beta}{\kappa_g} \sin(A) & -\frac{i\kappa}{\kappa_g} \sin(A) \\ -\frac{i\kappa}{\kappa_g} \sin(A) & \cos(A) - \frac{i\Delta\beta}{\kappa_g} \sin(A) \end{bmatrix} \begin{bmatrix} E_1(z_0) \\ E_2(z_0) \end{bmatrix} \quad (1)$$

Here κ is the coupling coefficient between the two waveguides, determined mainly by the distance between the cores. $\Delta\beta = \frac{\beta_1 - \beta_2}{2}$ denotes the detuning, or the phase mismatch parameter, which is determined by the propagation constants $\beta_{1,2}$ in the two constituent waveguides when uncoupled. Also, in (1), z represents the axial coordinate in the direction of propagation, z_0 is the point of entry into the coupler, $\kappa_g = \sqrt{\kappa^2 + \Delta\beta^2}$ is the generalized coupling coefficient, and $A = \int_{z_0}^z \kappa_g dz = \kappa_g (z - z_0)$ is the integral of the generalized coupling coefficient, also referred to as the ‘pulse area’.

In the design of robust composite-section directional couplers, several segments of uniform waveguides widths and uniform gaps are concatenated together, such as to achieve better robustness for a specific error model. Each uniform section is described by its own unitary matrix. We relate to variations in the operating wavelength first. To realize couplers with reduced spectral sensitivity, we utilize the first-order scheme [14], in which the second-order derivative with respect to pulse area error is nullified, as defined in equation (2):

$$\frac{\partial^2}{\partial A^2} \left(\prod_i \hat{U}_i \right) = 0 \quad (2)$$

The solution of (2) for two segments, $i = 1, 2$, with full power swap ($|\hat{U}_{12}| = 1$), yields the following relations: $\kappa_1 = \kappa_2 = \kappa$, and $\Delta\beta_1 = -\Delta\beta_2 = \kappa$. The extraction of waveguides widths and lengths in each segment is detailed in Appendix A.

A two-section composite directional coupler is illustrated in Fig. 1. The coupler comprises one uniform waveguide and a second waveguide of position-dependent width. The second

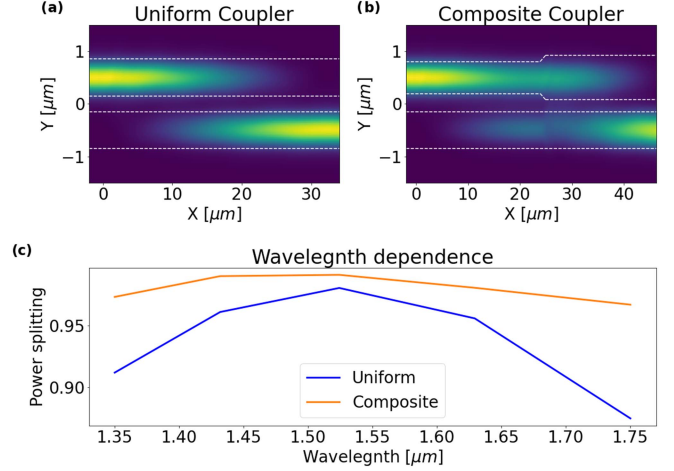


Fig. 2. Three-dimensional finite difference time domain simulations. Panels (a) and (b) Show the field propagation along devices. (a): A standard coupler comprised of two uniform ridge waveguides with 750 nm widths and 1 μm separation between their cores' centers. The ridges are defined in a 220 nm-thick device layer through partial etching to a depth of 77 nm between the waveguides and 85 nm to their sides. The coupler is 32.9 μm long. (b): A composite-sections coupler of dissimilar ridge waveguides with the same etching depths. One waveguide is uniform with 750 nm width. The width of the second waveguide varies between two sections of 24.39 μm and 21.83 μm lengths. The widths in the first and second sections are 660 nm and 890 nm, respectively. The separation between the centers of the two cores is fixed at 1 μm . The white dashed lines in panels (a) and (b) Mark the edges of the waveguide cores. (c): Calculated power splitting ratios of the uniform (blue) and composite-sections (orange) couplers as functions of wavelength. The composite sections coupler is less sensitive to wavelength variations.

waveguide consists of repeating sections of widths $W_{1,2}$ and length $L_{1,2}$. The lateral separation g between the centers of the two waveguides remains constant. To reduce scattering and reflection losses at abrupt width changes, a 1 μm long tapering region is inserted in each width transition.

To verify our design, a three-dimensional finite difference time domain (FDTD) simulation was performed with Lumerical, a commercially available solver. The simulation compared between uniform and composite-sections directional couplers of SOI ridge waveguides, designed nominally for complete power swap. The thickness of the silicon device layer is 220 nm and that of the buried oxide layer is 2 μm . The exact dimensions of waveguides within the couplers were taken from atomic force microscope measurements of fabricated devices (see next section). The depth of partial etching is 77 nm between the two ridge waveguides and 85 nm to their sides. The lateral separation between the centers of the two waveguides is fixed at 1 μm . Examples of the results of the field propagation are displayed in Fig. 2(a)–2(b).

The wavelength dependence of both couplers is shown in Fig. 2(c). The blue trace presents a 32.9 μm -long uniform coupler between waveguides of 750 nm widths. Corresponding results for a composite-sections coupler ($W_1 = 660$ nm, $W_2 = 890$ nm, $L_1 = 24.39$ μm , $L_2 = 21.83$ μm , overall length of 46.22 μm) are shown in orange. The composite-sections design reduces wavelength dependent errors in the coupling ratio from 10.6% to 2.4%. In addition, the propagation constants $\beta_{1,2}$, the

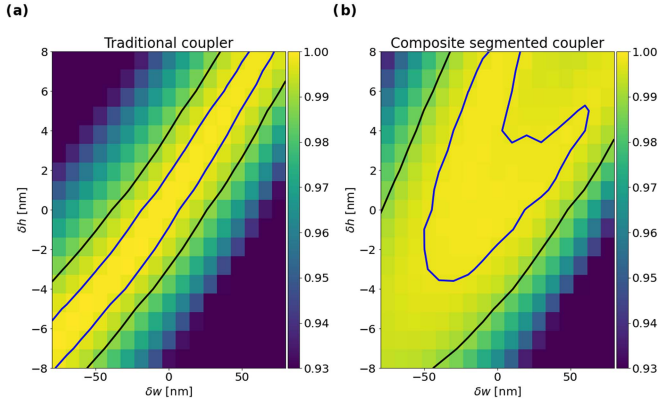


Fig. 3. Calculated power splitting ratios at 1550 nm wavelength of silicon-photonics directional couplers as functions of errors δh in the partial etching depth and errors δw in the widths of constituent ridge waveguides. The ridges are defined in a 220 nm-thick device layer through partial etching to a nominal depth of 70 nm. The black lines mark contours of splitting ratios 99% and higher, and the blue lines mark contours of 99.8% splitting ratios and higher. The errors δh and δw are not correlated, and both are common to the two waveguides throughout the coupler length. (a): Standard coupler comprised of two uniform ridge waveguides with a nominal width of 1200 nm and separation of 1550 nm between the cores' centers. The coupler is 157 μm long. (b): A composite-sections coupler of dissimilar ridge waveguides with the same etching depth. One waveguide is uniform, with a nominal 1200 nm width. The designed width of the second waveguides varies in three composite segments: 1135 nm width for 119 μm , 1200 nm width over 157 μm , and 1285 nm width for 101 μm . The separation between the centers of the two cores is again fixed at 1550 nm. The calculations suggest that the composite-sections coupler is more robust to real-world geometrical fabrication errors.

coupling coefficient κ and the mismatch parameter $\Delta\beta$ were calculated numerically for each waveguide segment, and the power splitting ratios of the directional couplers were found by applying (1) to each section. These approximate calculations were found to be in good agreement with the full FDTD simulation.

Next, we propose a composite-sections coupler design with increased tolerance to real-world geometric fabrication errors. The most commonly encountered deviations from design parameters are in the partial etching depth of ridge waveguides and in their widths. Both types of deviations are likely to be the same for the two constituent waveguides of a directional coupler, along its entire length. Errors in width and depth are statistically uncorrelated. Numerical analysis of modal solutions suggests that the detuning parameter $\Delta\beta$ is the most sensitive to geometrical errors. We therefore expanded (1) in terms of a Taylor series with respect to detuning errors $\delta\Delta\beta$. The composite-sections coupler was designed to nullify the detuning error $\delta\Delta\beta$ to the first order, while keeping the constraint for complete power swap, $|\hat{U}_{12}| = 1$. These considerations result in a three-section design, with the following relations among parameters:

$$\begin{aligned} \kappa_1 = \kappa_2 = \kappa_3 &\triangleq \kappa \\ -\Delta\beta_1 = \Delta\beta_3 = \kappa, \Delta\beta_2 &= 0 \end{aligned} \quad (3)$$

Fig. 3 shows the calculated splitting ratios at 1550 nm wavelength of two directional couplers, designed again for a complete power swap, as functions of width and etching depth errors. Panel (a) presents a standard coupler of uniform cross-section,

whereas panel (b) shows the results for a three-section composite coupler (for details of sections lengths and waveguides widths, see Fig. 3). Etching depth errors δh between ± 8 nm and width errors δw within ± 80 nm were considered. The analysis suggests that the composite-sections coupler is more robust to geometrical fabrication errors. The mean splitting ratio across all error values is 97.6% with deviations of +2.4% and -3.2% in the uniform coupler, compared to a mean 99.1% with deviations of +0.9% and -2.0% in the composite-sections coupler.

This design approach described above is suitable for arbitrary power splitting ratio, by setting the requirement for the propagator element as $|\hat{U}_{12}|^2 = \eta$. For example, a 50:50 power splitter ($\eta = 0.5$) with enhanced wavelength insensitivity can be obtained with the choice of [14]:

$$\begin{aligned} \kappa_1 = \kappa_2 &\triangleq \kappa \\ \Delta\beta_1 = -5.52\kappa, \Delta\beta_2 &= 0.69\kappa \\ A_1 = A_2 &= \frac{\pi}{2} \end{aligned} \quad (4)$$

III. DEVICE FABRICATION AND TESTING

To compare between uniform and composite-section couplers, test patterns of racetrack resonators were fabricated in standard SOI substrates. The lengths of the resonators were 1.3 mm. The widths of waveguides within the directional couplers forming the resonators, the separation between the waveguides, and the etching depths were the same as those in Fig. 2 above. A reference resonator device was based on a uniform coupler of 350 μm length. A second device included a composite-sections coupler with ten repeating periods. Following the ten periods, another composite section was added to provide critical coupling into the resonator. That section comprised of two segments, with the width of one waveguide fixed at 750 nm. The width of the other waveguide was 486 nm in the first section and 690 nm in the second. The lengths of the two sections were 11.6 μm and 32.86 μm , respectively. Long couplers were deliberately used in both the uniform and composite section designs, to enhance the wavelength dependence of their splitting ratios and compare their robustness. Errors in the long couplers are also indicative of the anticipated performance trends of multiple cascaded gates in more complex circuits.

Optical waveguides were defined in the silicon device layer using electron-beam lithography, followed by inductively coupled plasma reactive-ion etching. The etching process used a mixture of SF₆ and C₄F₈ gasses, at flow rates of 65 sccm and 10 sccm, respectively. Etching was carried out at a vacuum level of 4×10^{-10} bar and radio frequency power of 100 W at a 6 nm \times s⁻¹ rate. Fig. 4(a) shows a top-view optical microscope image of one resonator device. Fig. 4(b) presents a top view optical microscope image of one period within the composite-sections coupler. Figs 4(c)–4(e) show scanning electron microscope images of focused ion beam cross-sections of uniform and composite-section couplers.

Light was coupled between the bus waveguides of resonator devices and standard single-mode fibers using vertical grating couplers. The coupling losses were 10 dB per facet. Fig. 5(a)

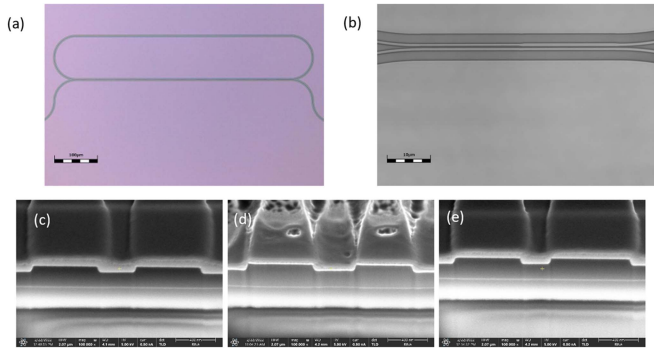


Fig. 4. Fabricated devices (a): Top-view optical microscope image of a silicon-photonic racetrack resonator device used in the comparison between uniform and composite-sections directional couplers. The scale bar represents $100\ \mu\text{m}$. (b): Top-view optical microscope image of one period within a long composite-sections directional coupler. The scale bar represents $10\ \mu\text{m}$. (c)-(e): Scanning electron microscope images of focused ion beam cross-sections of directional couplers. The scale bars represent $400\ \text{nm}$. (c): Uniform coupler with two identical waveguides, each $750\ \text{nm}$ wide. (d): The first section of a composite-sections coupler, in which the width of the right waveguide is reduced to $660\ \text{nm}$. (e): The second section of a composite coupler, in which the width of the right waveguide is increased to $890\ \text{nm}$.

shows optical vector network analyzer measurements of the normalized transfer functions of optical power through the two devices. The wavelength resolution was $3\ \text{picometers}$. The transfer functions consist of multiple periods with a free spectral range of $0.5\ \text{nm}$. The Q factors of both resonators are 30000 . The use of composite-sections couplers did not lead to measurable excess losses. The extinction ratios of the periodic transmission notches of the uniform-coupler device vary strongly across the C-band wavelengths range, between $0.25\ \text{dB}$ and $20\ \text{dB}$. By contrast, the extinction ratios of the resonator with the composite-sections coupler remained within $16 \pm 3\ \text{dB}$ over the entire wavelength range.

Fig. 5(b) presents the power splitting ratios of the two couplers as functions of wavelengths, as calculated from the observed extinction ratios of the two transfer functions [5]. The splitting ratio of the long, uniform coupler varies between 0.3 and 1 , whereas that of the composite-sections coupler remains within 0.34 ± 0.02 . The results illustrate the superior robustness of the composite-sections design with respect to wavelength changes, in agreement with analysis [14]. Fig. 5(b) also presents the calculated splitting ratios of both directional couplers as functions of wavelengths, based on (1). Contributions of transition regions leading the two waveguides to and from the coupling region were accounted for as well. Agreement between models and measurements of splitting ratios is very good.

IV. SUMMARY

In this work, we have proposed and demonstrated fault-tolerant directional couplers comprised of sections with different waveguides widths. The design concept is inspired by the principles of composite pulses in atomic physics [15], [16], which were recently expanded by the detuning modulated composite sequence scheme to tackle errors in PICs [14]. This

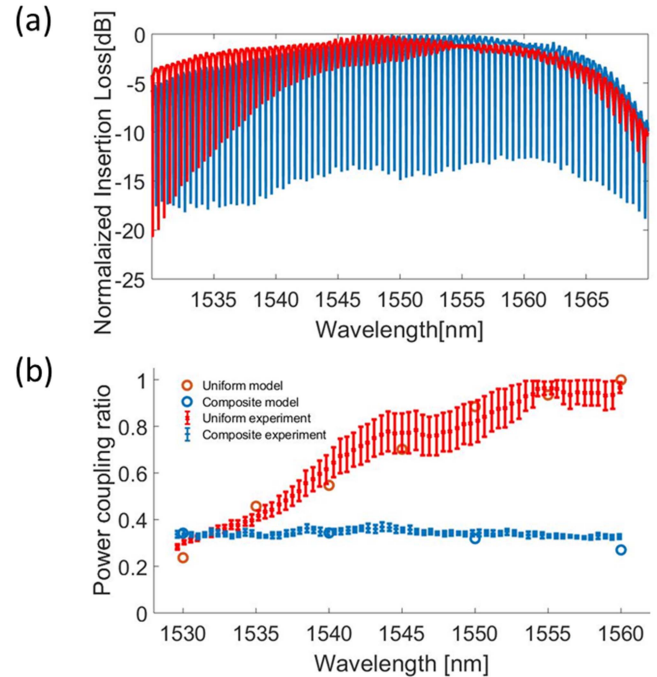


Fig. 5. (a): Measured transfer functions of optical power through two racetrack resonator devices in silicon-on-insulator, as functions of wavelength. Red: A reference device comprised of a long uniform directional coupler. Blue: Device based on a long composite-sections directional coupler. The reference device exhibits strong variations in extinction ratios of periodic transmission notches across the C-band wavelengths. The extinction ratios of the composite-sections coupler device remain more uniform across the same wavelength range. (b): Power splitting ratios of the two-directional couplers, based on the measured extinction ratios of panel (a) (same colors, see legend). The composite-sections design reduces the wavelength variations of the coupler splitting ratio by a factor of 15 . The splitting ratios agree well with calculations based on (1).

study shows that the scheme developed for a general quantum system is also applicable to integrated optics. The results suggest a considerable improvement in the robustness of single-qubit state manipulation in the common path encoding of photonic qubits.

We have experimentally demonstrated the enhanced wavelength insensitivity of a full swap coupler. Compared with a reference uniform device, splitting ratio variations of a long composite-sections coupler across the C-band were reduced fifteen-fold. Measurements and calculations were in good agreement. The results suggest a large potential benefit in the cascaded operation of multiple couplers in series within larger processing layouts. A second design targeted common errors in both waveguides width and etching depth within the coupler. The width and depth errors for which the splitting ratio remains above 99% were calculated for a reference uniform coupler and a composite coupler. The composite coupler design tolerates geometrical errors that are twice larger.

The design concept shows great promise for enabling and scaling integrated photonic quantum information processors, which will require many single-qubit operations in every architecture. While this design can eliminate errors to the first order, the concept can be extended to mitigate second and higher-order errors as well. Additional extensions of this scheme

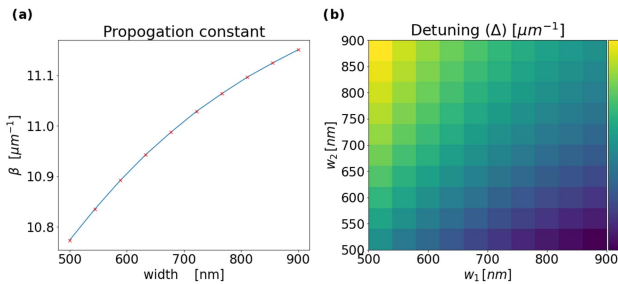


Fig. 6. (a): Calculated propagation constant of a single uncoupled ridge waveguide as a function of its width, at 1550 nm wavelength. The thickness of the silicon device layer was 220 nm and the depth of partial etching to the side of the ridge core was 70 nm. (b) Calculated detuning in propagation constants between two waveguides of widths $w_{1,2}$ at 1550 nm wavelength. The detuning is given by half the difference between the propagation constants of the uncoupled modes of each waveguide.

would address the design of robust single- and two-qubit unitary gates.

APPENDIX A – INVERSE DESIGN FOR COUPLED WAVEGUIDES

The general framework presented in this work is valid for every two-level system that exhibits the same dynamics as given in (1). The first-order solution presented in this paper, $\kappa_1 = \kappa_2 = \kappa$ and $\Delta\beta_1 = -\Delta\beta_2 = \kappa$, would nullify the second-order derivative of the transfer function and result in robust population transfer for each such system. In this appendix we address the problem of inverse design: calculating the required waveguides widths, gaps, and lengths of coupler segments that realize the required values of κ , $\Delta\beta$.

According to the coupled-mode theory, the detuning $\Delta\beta$ equals half the difference between the propagation constants of the uncoupled modes in each waveguide. Since there is no analytic solution for the propagation constant as a function of width for ridge waveguides, we performed a numerical simulation using Lumerical, a commercially available solver, and extracted the propagation constant as a function of width. We then interpolated the calculated data to identify the waveguide width corresponding to a specific detuning value. An example is presented in Fig. 6.

The coupling coefficient κ is determined by the overlap integral between the transverse profiles of the two modes, and it decays exponentially with the separation between the waveguides cores centers. The coefficient is given by half the difference between the propagation constants β_{\pm} of the two super-modes that are guided by the dual-waveguide structure. The propagation constants β_{\pm} and the coupling coefficient κ were obtained through numerical solutions as above. Fig. 7 shows an example of the calculated results as a function of cores separation, for waveguides of 700 nm width and 1550 nm wavelength. The dependence of κ on the cores' separation is well described by an exponential fit.

In this work, we have chosen for simplicity to maintain a constant separation of 1 μm between the cores' centers. In this manner, the coupling coefficient κ was nearly the same in both sections. We also defined a constant width $w_1 = 750$ nm for one

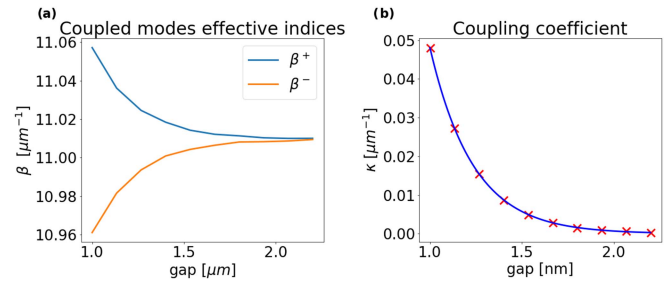


Fig. 7. (a): Calculated propagation constants of the symmetric (blue) and anti-symmetric (red) coupled modes in a directional coupler as a function of the separation between the centers of ridge waveguides cores. The widths of the two waveguides were both 700 nm, and the wavelength was 1550 nm. (b) Calculated coupling coefficient as a function of the separation between the cores of the same two waveguides (red markers). The solid line presents an exponential fit.

of the ridge waveguides. The width of the second waveguide w_2 was varied to obtain $\Delta\beta_1 = -\Delta\beta_2 = \kappa$. The pulse area for a uniform section is given by $A = \int_{z_0}^z \kappa_g dz = \kappa_g L$, where $\kappa_g = \sqrt{\kappa^2 + \Delta\beta^2}$. The length of the section is chosen by dividing the required pulse area by the generalized coupling coefficient κ_g .

REFERENCES

- [1] Y. A. Vlasov, "Silicon CMOS-integrated nano-photonics for computer and data communications beyond 100G," *IEEE Commun. Mag.*, vol. 50, no. 2, pp. s67–s72, Feb. 2012, doi: [10.1109/MCOM.2012.6146487](https://doi.org/10.1109/MCOM.2012.6146487).
- [2] J. Wang, F. Sciarrino, A. Laing, and M. G. Thompson, "Integrated photonic quantum technologies," *Nature Photon.*, vol. 14, pp. 273–284, 2020, doi: [10.1038/s41566-019-0532-1](https://doi.org/10.1038/s41566-019-0532-1).
- [3] T. Rudolph, "Why I am optimistic about the silicon-photonics route to quantum computing," *APL Photon.*, vol. 2, 2017, Art. no. 030901, doi: [10.1063/1.4976737](https://doi.org/10.1063/1.4976737).
- [4] X. Qiang *et al.*, "Large-scale silicon quantum photonics implementing arbitrary two-qubit processing," *Nature Photon.*, vol. 12, pp. 534–539, 2018, doi: [10.1038/s41566-018-0236-y](https://doi.org/10.1038/s41566-018-0236-y).
- [5] W. Bogaerts *et al.*, "Silicon microring resonators," *Laser Photon. Rev.*, vol. 6, pp. 47–73, 2012, doi: [10.1002/lpor.201100017](https://doi.org/10.1002/lpor.201100017).
- [6] M. A. Nielsen and I. L. Chuang, *Quantum Computation and Quantum Information*, Cambridge, U.K.: Cambridge Univ. Press, 2010, doi: [10.1017/cbo9780511976667](https://doi.org/10.1017/cbo9780511976667).
- [7] J. Wang *et al.*, "Multidimensional quantum entanglement with large-scale integrated optics," *Science*, vol. 360, pp. 285–291, 2018, doi: [10.1126/science.aar7053](https://doi.org/10.1126/science.aar7053).
- [8] M. Gimeno-Segovia, P. Shadbolt, D. E. Browne, and T. Rudolph, "From three-photon Greenberger-Horne-Zeilinger states to ballistic universal quantum computation," *Phys. Rev. Lett.*, vol. 115, 2015, Art. no. 020502, doi: [10.1103/PhysRevLett.115.020502](https://doi.org/10.1103/PhysRevLett.115.020502).
- [9] R. Santagati *et al.*, "Silicon photonic processor of two-qubit entangling quantum logic," *J. Opt.*, vol. 19, 2017, Art. no. 114006, doi: [10.1088/2040-8986/aa8d56](https://doi.org/10.1088/2040-8986/aa8d56).
- [10] Z. Lu *et al.*, "Broadband silicon photonic directional coupler using asymmetric-waveguide based phase control," *Opt. Exp.*, vol. 23, pp. 3795–3808, 2015, doi: [10.1364/oe.23.003795](https://doi.org/10.1364/oe.23.003795).
- [11] H. Yun, L. Chrostowski, and N. A. F. Jaeger, "Ultra-broadband 2×2 adiabatic 3 dB coupler using subwavelength-grating-assisted silicon-on-insulator strip waveguides," *Opt. Lett.*, vol. 43, no. 8, pp. 1935–1938, 2018, doi: [10.1364/OL.43.001935](https://doi.org/10.1364/OL.43.001935).
- [12] D.-X. Xu *et al.*, "High bandwidth SOI photonic wire ring resonators using MMI couplers," *Opt. Exp.*, vol. 15, no. 6, pp. 3149–3155, 2007, doi: [10.1364/OE.15.003149](https://doi.org/10.1364/OE.15.003149).
- [13] H. Guan *et al.*, "Passive silicon ring-assisted Mach-Zehnder interleavers operating in the broadband spectral range," *Appl. Opt.*, vol. 59, no. 27, pp. 8349–8354, 2020, doi: [10.1364/AO.396472](https://doi.org/10.1364/AO.396472).

- [14] E. Kyoseva, H. Greener, and H. Suchowski, "Detuning-modulated composite pulses for high-fidelity robust quantum control," *Phys. Rev.* vol. 100, 2019, Art. no. 032333, doi: [10.1103/PhysRevA.100.032333](https://doi.org/10.1103/PhysRevA.100.032333).
- [15] A. J. Shaka, "Composite pulses for ultra-broadband spin inversion," *Chem. Phys. Lett.*, vol. 120, pp. 201–205, 1985, doi: [10.1016/0009-2614\(85\)87040-8](https://doi.org/10.1016/0009-2614(85)87040-8).
- [16] E. L. Hahn, "Spin echoes," *Phys. Rev.*, vol. 80, pp. 580–594, 1950, doi: [10.1103/PhysRev.80.580](https://doi.org/10.1103/PhysRev.80.580).

Moshe Katzman received the B.Sc. and M.Sc. degrees in electrical engineering in 2015 and 2017, respectively, from Bar-Ilan University, Ramat Gan, Israel, where he is currently working toward the Ph.D. degree in electrical engineering.

His research interests include the development of hybrid-silicon photonics fabrication and measurements techniques, nonlinearities of chalcogenide glasses, and surface acoustic waves in silicon photonics.

Yonatan Piasetzky received the B.Sc. degree in physics and electrical engineering from Tel-Aviv University, Tel Aviv, Israel, in 2016, and the M.Sc. degree in physics from the Weizmann Institute of Science, Rehovot, Israel, in 2019. He is currently working toward the Ph.D. degree in physics with Tel-Aviv University.

His research interests include quantum information processing and communications in integrated optical devices.

Evyatar Rubin is currently working toward the B.Sc. degree in electrical engineering and physics with Bar-Ilan University, Ramat-Gan, Israel.

His research focuses on the modeling of silicon photonic devices.

Ben Barenboim is currently working toward the B.Sc. degree in electrical engineering and physics with Bar-Ilan University, Ramat-Gan, Israel.

His research focuses on the modeling of silicon photonic devices.

Maayan Priel received the B.Sc. and M.Sc. degrees in chemistry, in 2015 and 2017, respectively from Bar-Ilan University, Ramat Gan, Israel, where she is currently working toward the Ph.D. degree in electrical engineering.

Her current research interests include fabrication and measurements of passive and active silicon photonic devices, surface acoustic wave-photonic devices, and microwave photonics.

Muhammed Erew received the B.Sc. degree in physics, the B.Sc. degree in electrical engineering, and the M.Sc. degree in physics in 2013, 2013, and 2020, respectively, from Tel-Aviv University, Tel-Aviv, Israel, where he is currently working toward the Ph.D. degree in physics.

His research interests include optical quantum computing and error corrections in one-way quantum computing and in surface codes.

Avinoam (Avi) Zadok received the Ph.D. degree in electrical engineering from Tel-Aviv University, Tel-Aviv, Israel, in 2008. Between 2007 and 2009, he was a Postdoctoral Research Fellow with the Department of Applied Physics, California Institute of Technology, Pasadena, CA, USA. In 2009, he joined the Faculty of Engineering, Bar-Ilan University, Ramat-Gan, Israel, where he has been a Full Professor since 2017.

Dr. Zadok is a coauthor of 160 papers in scientific journals and reviewed proceedings of international conferences. His research interests include fiber-optics, nonlinear optics, integrated photonic devices, and opto-mechanics. Dr. Zadok was the recipient of the Krill Award of the Wolf Foundation in 2013, Starter Grant from the European Research Council in 2015, and Consolidator Grant from the same agency in 2020. Dr. Zadok was a Member of the Israel Young Academy during 2016–2020 and was its chairman for 2019–2020.

Haim Suchowski received the B.A. degree in physics and the B.Sc. degree in electrical engineering from Tel Aviv University, Tel Aviv, Israel, in 2004 and 2004, respectively, and the M.Sc. and Ph.D. degrees in physics from the Weizmann Institute of Science, Rehovot, Israel, in 2006 and 2011, respectively. Between 2011 and 2014, he performed his postdoctoral research with the University of California, Berkeley, CA, USA. In 2014, he joined Tel Aviv University and he has been an Associate Professor since 2018.

He has authored or coauthored 54 articles and was awarded 13 patents. His research interests include ultrafast dynamics in condensed matter physics, plasmonic nanostructures, and 2D materials. He also performs research in quantum integrated photonics and nonlinear optics. He was the recipient of the Fulbright postdoctoral fellowship in 2012, Alon Award for young scientists in 2015, and Starter Grant from the European Research Council in 2014.